Gondwana Research 60 (2018) 94–104

Contents lists available at ScienceDirect

Gondwana Research

journal homepage: www.elsevier.com/locate/gr

Late Cretaceous to early Eocene deformation in the northern Tibetan Plateau: Detrital apatite fission track evidence from northern Qaidam basin

Xing Jian [a,*], Ping Guan [b], Wei Zhang [a], Hanghai Liang [a], Fan Feng [c], Ling Fu [d]

[a] State Key Laboratory of Marine Environmental Science, College of Ocean and Earth Sciences, Xiamen University, Xiamen 361102, PR China
[b] MOE Key Laboratory of Orogenic Belts and Crustal Evolution, School of Earth and Space Sciences, Peking University, Beijing 100871, PR China
[c] Petroleum Exploration and Production Research Institute, Sinopec, Beijing 100083, PR China
[d] Research Institute of Petroleum Exploration and Development (RIPED), PetroChina, Beijing 100083, PR China

A R T I C L E I N F O

Article history:
Received 14 September 2017
Received in revised form 21 March 2018
Accepted 6 April 2018
Available online 04 May 2018

Handling Editor: A.S. Collins

Keywords:
Detrital thermochronology
Apatite
Provenance
Exhumation
Qaidam basin

A B S T R A C T

Unraveling the growth of northern Tibet is crucial to understanding the geodynamic processes of the India-Eurasia collision, evaluating plateau uplift models and reconstructing associated paleoclimate history. However, pre-middle Miocene deformation history of northern Tibet remains poorly understood. We use detrital apatite fission track (detrital AFT) thermochronology of Mesozoic and Cenozoic sedimentary rocks from northern Qaidam basin to constrain the early growth of northern Tibet. Detrital AFT ages of the Mesozoic samples are younger than their depositional ages, indicating that the Mesozoic succession underwent two stages of exhumation after deep burial during 80–61 Ma and 54–47 Ma. Detrital AFT ages of the Cenozoic samples are older than their depositional ages and reveal that their source region experienced two periods of exhumation (peak ages in 86–59 Ma and 54–36 Ma). These results suggest that the northern Tibet successively experienced Late Cretaceous–early Paleocene and early–middle Eocene deformation. The Late Cretaceous–early Paleocene deformation implies that the extent of pre-collisional (India-Eurasia) deformation region in the plateau were much larger than previously known. The static detrital AFT peak ages (54–51 Ma) based on lag-time analysis for the Paleogene samples demonstrate the early Eocene deformation was a rapid and short-lived event, which was a far-field response to the India-Eurasia collision. Hence, we advocate synchronous deformation throughout the northern plateau at the collision time. Lag-time analysis results also demonstrate absence of Oligocene to early Miocene cooling ages and post-Eocene decreasing exhumation rates in the Cenozoic source regions. This suggests relatively quiescent tectonic settings in the Qilian Mountains during the Oligocene–early Miocene and agrees that the lateral strike-slip movement of the Altyn Tagh Fault was accommodated out of the plateau by the end of the early Miocene.

1. Introduction

As the world's highest and most extensive plateau (Fig. 1A), Tibet is an ideal field laboratory for understanding geodynamic processes of continental collision and interactions between plateau uplift and global climate (Harrison et al., 1992; Molnar et al., 1993; Ruddiman et al., 1997). Early models of Tibetan Plateau formation assumed that the India-Eurasia collision at ca. 55–50 Ma (Najman et al., 2010; Van Hinsbergen et al., 2012) was the major force of deformation and crustal thickening, and post-collision convergence between the two plates doubled the thickness of the crust and created much of the current high topography (England and McKenzie, 1982; England and Houseman, 1986; Tapponnier et al., 2001). Given that the India plate, as a rigid indenter, converges with a weaker Eurasian lithosphere since the collision, most of these models advocated northward and eastward propagating of strain in the plateau. In this case, deformation and high-relief topography were supposed to occur earliest near the plate boundary, whereas the northern Tibet deformation was young (e.g., England and Houseman, 1986; Zheng et al., 2000; Tapponnier et al., 2001).

New data challenge this idea. First, numerous studies find that deformation and considerable crustal thickening had already occurred in the southern and central Tibetan Plateau prior to the India-Eurasia collision (e.g., Murphy et al., 1997; Kapp et al., 2005, 2007; Volkmer et al., 2007; Rohrmann et al., 2012; Ding et al., 2014). Several similarities can be drawn between the pre-collisional tectonic setting of the Tibetan Plateau and of the modern Altiplano of the Andes (Kapp et al., 2005; Lippert et al., 2014), where eastward subduction of the Nazca plate has resulted in thickened South American lithosphere and an associated high-elevation mountain belt. The modern central Andes may act as an

* Corresponding author.
E-mail address: xjian@xmu.edu.cn (X. Jian).

https://doi.org/10.1016/j.gr.2018.04.007
1342-937X/

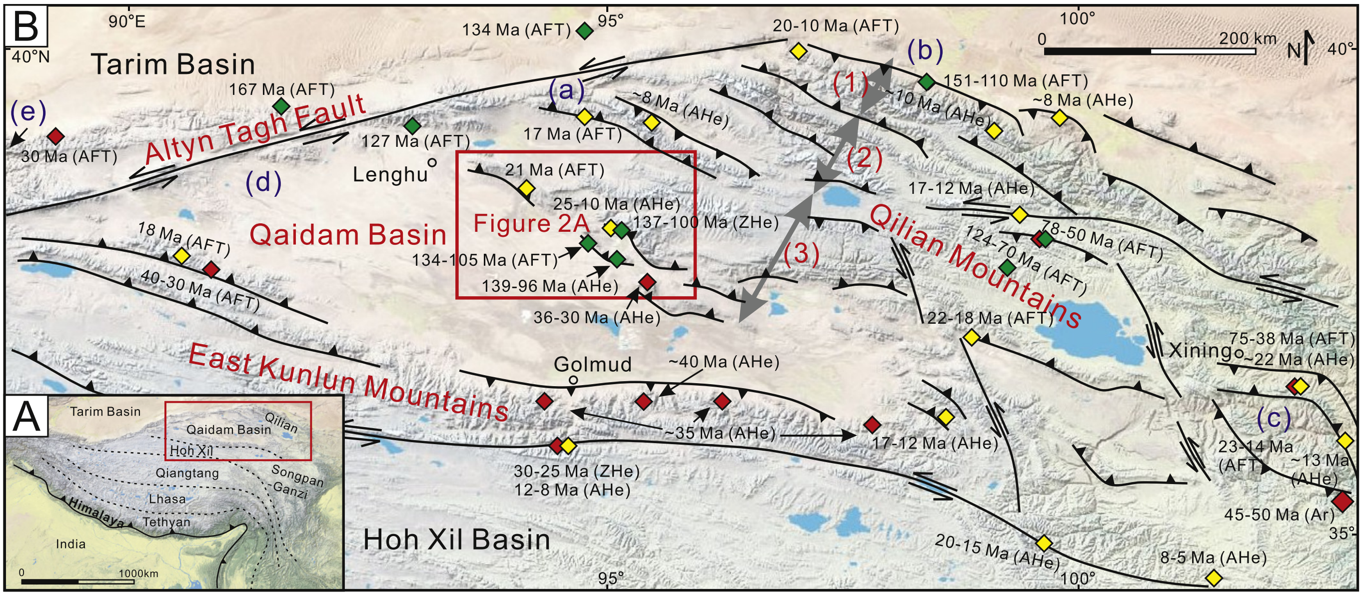

Fig. 1. (A) Location of the Qaidam basin. (B) Major tectonic elements in northern Tibet and previous low-temperature thermochronology (diamond) and detrital thermochronology (lowercase letters) study sites. Previous detrital thermochronology studies on northern Tibet include the following Cenozoic sedimentary basins: (a) Subei basin (Lin et al., 2015), (b) Jiuxi basin (W. Wang et al., 2016), (c) Xining-Guide basin (X. Wang et al., 2016), (d) Western Qaidam basin (Wang et al., 2015) and (e) southern Tarim basin (Yin et al., 2002). Basement thermochronological data are from George et al. (2001), Jolivet et al. (2001), Clark et al. (2010), Zheng et al. (2010), Duvall et al. (2011, 2013), Lease et al. (2011), Lu et al. (2012), Qi et al. (2016), F. Wang et al. (2016), Liu et al. (2017) and Zhuang et al. (2018). Green, red and yellow diamonds indicate pre-Cenozoic, Paleogene and Neogene cooling ages, respectively. AHe: apatite (U-Th)/He; AFT: apatite fission track; ZHe: zircon (U-Th)/He; Ar: $^{40}Ar/^{39}Ar$ of fault gouge. Gray double-headed arrows (1), (2) and (3) represent areas of North Qilian, Central Qilian and South Qilian-North Qaidam belts, respectively. (For interpretation of the references to color in this figure legend, the reader is referred to the web version of this article.)

analogue for the early growth history of the Tibet, where most of the plateau developed above an oceanic subduction zone in the absence of a continent-continent collision (e.g., Ding et al., 2014; Lippert et al., 2014). Thus, the southern margin of the Eurasian plate was inferred as an Andean-type margin since the Late Cretaceous (Staisch et al., 2016 and figures therein).

Second, although many structures on the north margin initiated since the middle–late Miocene (e.g., George et al., 2001; Lu and Xiong, 2009; Zheng et al., 2010; Duvall et al., 2013; Chang et al., 2015), recently published thermochronological data from East Kunlun and West Qinling orogenic belts (Clark et al., 2010; Duvall et al., 2011; F. Wang et al., 2016) and basin analysis results (e.g., Dupont-Nivet et al., 2004; Yin et al., 2008a; Zhuang et al., 2011) suggest that extensive deformation occurred across the northern Tibet during the Eocene, i.e., shortly after the India-Eurasia collision. However, Cenozoic deformation and uplift history of northern Tibet remains controversial. Potential deformation scenarios mainly include (A) synchronous widespread crustal shortening soon after collision (Clark, 2012), or (B) northward propagating shortening within northern Tibet (Wang et al., 2008; W. Wang et al., 2016). Furthermore, thermal modeling of (U–Th)/He age-elevation data show high relief (~1.82 times the relief of the present) during the middle Eocene (ca. 40 Ma) (F. Wang et al., 2016); however, paleoaltimetry results indicate that low to moderate elevations (<2000 m) persisted until the late Eocene and the northern Tibet achieved most of today's elevation after the middle Miocene (Polissar et al., 2009; Sun et al., 2015; Miao et al., 2016).

The Qaidam basin is the largest intracontinental basin in Tibetan Plateau (Fig. 1A). The basin contains a remarkably thick (3–16 km) Mesozoic–Cenozoic sedimentary succession, which potentially preserves substantial information about the tectonic evolution of northern Tibet (e.g., Ritts and Biffi, 2001; Yin et al., 2002, 2008b; Zhuang et al., 2011; Guan and Jian, 2013). Much remains to be understood about what happened within and adjacent to the Qaidam basin along with early deformation of northern Tibet. Detrital thermochronology allows studying long-term record of orogenic exhumation and getting thermal information of previously exposed bedrock. In this study, we present detrital apatite fission track (detrital AFT) data and interpretations for Jurassic, Early Cretaceous and Cenozoic sedimentary rocks in the northern Qaidam basin to determine the early exhumation history and deformation of northern Tibet.

2. Geological setting

The Qaidam basin is bounded by three large mountain ranges that reach elevations of up to 5 km. To the south are the East Kunlun Mountains, which separate the Qaidam basin from the Hoh Xil basin (Fig. 1A). The East Kunlun Mountains are dominantly composed of Early Cambrian to Early Devonian and Late Permian to Triassic igneous rocks and Devonian to Early Triassic marine sedimentary rocks (Dai et al., 2013; Huang et al., 2014), which are considered to be records of successive subduction-closure of Proto-Tethys and Paleo-Tethys oceans during the Paleozoic to early Mesozoic (Li et al., 2013; Cheng et al., 2017). The East Kunlun subsequently experienced late Mesozoic to Cenozoic multi-phase deformation and uplift events (Clark et al., 2010; Dai et al., 2013; Duvall et al., 2013; F. Wang et al., 2016; Fig. 1B).

The Qilian Mountains are to the east as a ca. 300 km wide fold-thrust belt (Fig. 1A) and from north to south consist of the North Qilian early Paleozoic complex, the Central Qilian Proterozoic basement and the South Qilian-North Qaidam metamorphic belt (Gehrels et al., 2003). This orogen is mainly composed of different types of metamorphic rocks, volcanic rocks, marine sedimentary strata as well as ophiolite associations (Gehrels et al., 2003). It is thought to be a suture zone conjunction of two continents between segments of Rodinia supercontinent and North China Craton. It preserves a complete history from continental breakup to ocean basin evolution (so-called Qilian Ocean), and to the ultimate continental collision during the Neoproterozoic to late Paleozoic (Song et al., 2013 and references therein).

To the northwest are Altun Mountains, which are created by an active left-lateral strike-slip fault (Altyn Tagh Fault) and separate the Qaidam basin from the Tarim basin (Fig. 1A). The Altun Mountains mainly consist of Archean-Proterozoic basement rocks and marine sedimentary strata, Paleozoic metamorphic and igneous rocks and Mesozoic sedimentary strata (Gehrels et al., 2003). The Cenozoic deformation of the Altun Mountains initiated at ca. 49 Ma (Yin et al., 2002) with movement on the left-lateral Altyn Tagh Fault and lateral extrusion before ca. 15 Ma, and crustal thickening and substantial uplift after ca. 15 Ma (Yue and Liou, 1999; Yue et al., 2003; Lu et al., 2016).

The Qaidam basin is situated approximately 2.7–3.0 km above sea level and covers approximately 120,000 km^2 (Fig. 1B). It is well accepted that the Mesozoic Qaidam basin was a foreland basin (Ritts and Biffi, 2001; Xia et al., 2001). The Cenozoic Qaidam basin was created by the development of a large synclinorium (Bally et al., 1986), which is closely associated with the continuous convergence between Indian and Eurasian plates and the uplift of northern Tibet (Tapponnier et al., 2001; Yin et al., 2008a, 2008b). The Mesozoic and Cenozoic sedimentary succession of the Qaidam basin was mainly deposited in a fluvial-lacustrine environment (e.g., Ritts and Biffi, 2001; Zhuang et al., 2011; Jian et al., 2014). Fig. 2B shows the stratigraphic and age framework of the sedimentary succession. Lithology and depositional environment descriptions of each stratigraphic unit are in Jian et al. (2013b).

3. Sampling and analytical methods

Paleocurrent orientation data were collected from the Cenozoic Yingchaogou (YCG) section and were mainly determined by ripple foresets and gravel imbrications. Six Jurassic, two Cretaceous and seven Cenozoic sandstone samples were collected from 4 outcrops (YCG, Jielvsu (JLS), Lulehe (LLH) and Dameigou (DMG) sections) and 2 Drill holes (Wells X9 and B1) for detrital thermochronology (Fig. 2). Sample descriptions are in Table 1. These samples were first crushed, and detrital apatite grains were separated using heavy liquids and standard magnetic separation techniques and were picked under a microscope.

Apatite fission track analyses were carried out at the State Key Laboratory of Earthquake Dynamics, China Earthquake Administration. All samples were dated by the external detector method (Gleadow and Duddy, 1981). Apatite grains were etched in 5.5 M nitric acid at 21 °C for 20 s. Apatite samples, the low-U mica external detectors and CN5 grass dosimeter were packaged together and were subsequently irradiated at China Institute of Atomic Energy, Beijing. The mica external detectors were etched with 21 °C in 40% hydrofluoric acid for 40 min. Fission track analyses were performed on a Zeiss Axioplan 2 microscope, by using dry objectives with magnification of 1000. Fission track ages were calculated by the zeta calibration method (Hurford and Green, 1983). The results are given in Table 1.

4. Results

Detrital AFT ages of the fifteen samples are between 80.5 ± 3.9 and 46.5 ± 2.3 Ma (Figs. 3–5; Table 1). The detrital AFT ages of all the Mesozoic samples pass X^2 test (i.e. P (X^2) > 5%), implying that all single-crystal ages represent a single population of ages for each sample. The Early Jurassic Sample DMG-13 shows a detrital AFT age of 61.6 ± 3.3 Ma, the Middle Jurassic Samples JLS-07 and LLH-04 have detrital AFT ages of 68.5 ± 3.9 Ma and 69.1 ± 3.3 Ma, respectively, while the Late Jurassic Samples DMG-31, JLS-11 and LLH-08 have relatively broad ages, i.e., 80.5 ± 3.9 Ma, 78.1 ± 4.4 Ma and 46.5 ± 2.3 Ma,

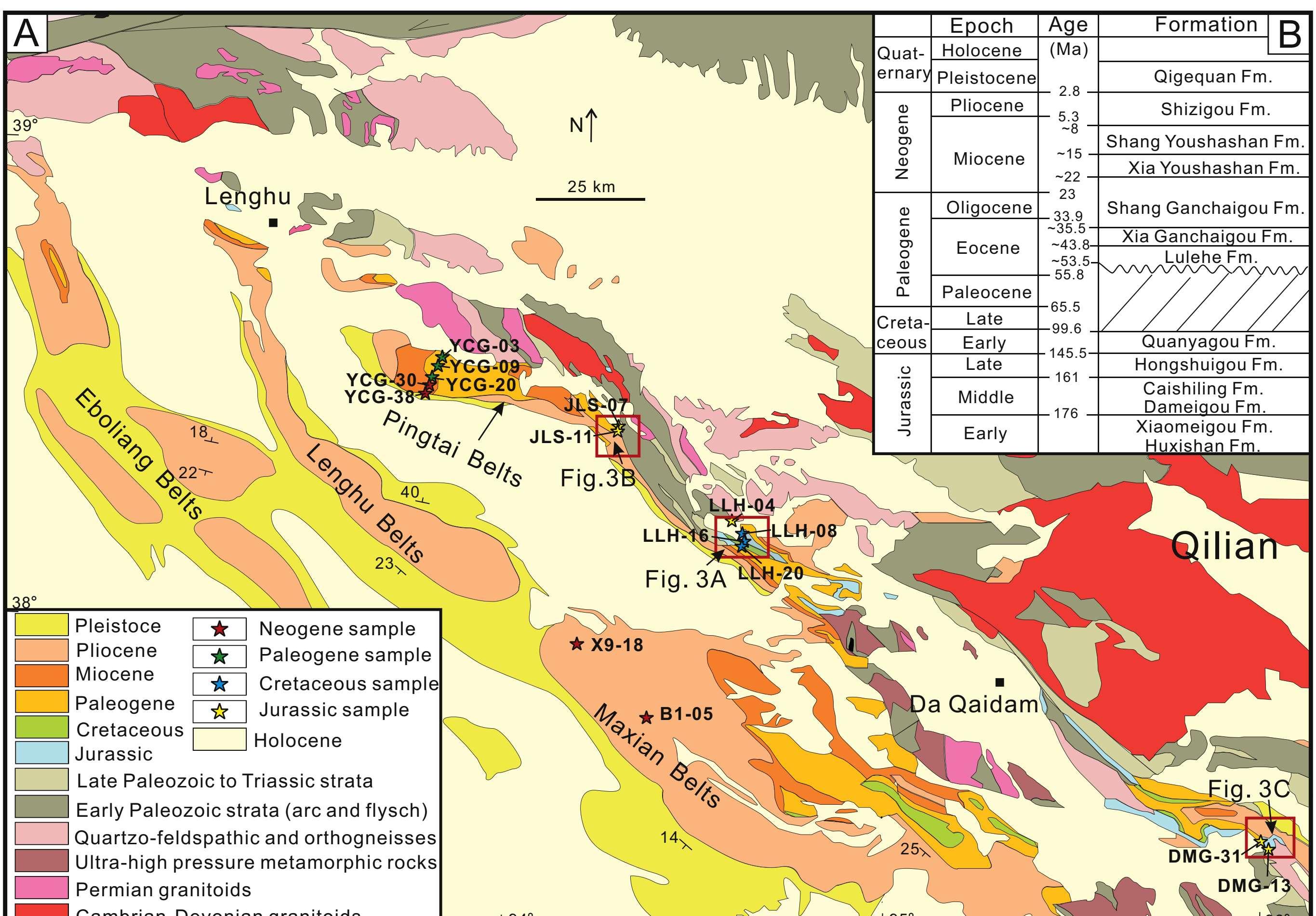

Fig. 2. (A) Simplified geologic map of the northern Qaidam basin and sample locations; (B) Mesozoic–Cenozoic stratigraphic framework.

Table 1
Sample descriptions and detrital apatite fission track analysis data.

Sample	Location	Depositional epoch	Formation	Nc	ρ_d (N_d)	ρ_s (N_s)	ρ_i (N_i)	U (ppm)	P (X^2) %	AFT age[a] (Ma ± 1σ)	Mean length (μm ± 1σ)	Std. dev. (μm)
DMG-13	37°36′55″N, 96°1′18″E	Early Jurassic	Xiaomeigou Fm.	30	0.926 (2315)	5.109 (820)	1.349 (2165)	18.2	36.6	61.6 ± 3.3	14.09 ± 0.09	0.87
JLS-07	38°24′19″N, 94°17′21″E	Middle Jurassic	Dameigou Fm.	30	0.805 (2013)	4.456 (753)	0.919 (1553)	14.3	20.3	68.5 ± 3.9	14.22 ± 0.11	1.1
LLH-04	38°10′54″N, 94°38′29″E	Middle Jurassic	Dameigou Fm.	30	0.896 (2239)	9.183 (1483)	2.090 (3376)	29.2	21.6	69.1 ± 3.3	14.23 ± 0.09	0.91
JLS-11	38°24′16″N, 94°17′9″E	Late Jurassic	Hongshuigou Fm.	30	0.790 (1976)	3.599 (835)	0.639 (1482)	10.1	83.7	78.1 ± 4.4	14.05 ± 0.10	0.96
LLH-08	38°10′9″N, 94°38′44″E	Late Jurassic	Hongshuigou Fm.	30	0.881 (2202)	7.589 (1089)	2.528 (3628)	35.9	60.4	46.5 ± 2.3	14.00 ± 0.10	1.07
DMG-31	37°31′35″N, 96°0′22″E	Late Jurassic	Hongshuigou Fm.	28	0.911 (2277)	7.748 (1352)	1.539 (2685)	21.1	86.6	80.5 ± 3.9	14.38 ± 0.09	0.96
LLH-16	38°9′40″N, 94°38′30″E	Early Cretaceous	Quanyagou Fm.	30	0.866 (2164)	4.705 (687)	1.421 (2075)	20.5	65.9	50.4 ± 2.9	14.09 ± 0.12	1.21
LLH-20	38°9′39″N, 94°38′29″E	Early Cretaceous	Quanyagou Fm.	29	0.850 (2126)	4.655 (810)	1.286 (2237)	18.9	12	54.1 ± 2.9	13.91 ± 0.11	1.07
YCG-03	38°30′N, 93°55′44″E	Middle Eocene	Xia Ganchaigou Fm.	30	0.775 (1938)	3.773 (949)	1.003 (2522)	16.2	92.2	51.3 ± 2.7	14.42 ± 0.11	1.15
YCG-09	38°29′30″N, 93°55′30″E	Late Eocene	Xia Ganchaigou Fm.	29	0.760 (1900)	2.946 (960)	0.731 (2383)	12	53.8	53.8 ± 2.8	13.38 ± 0.11	1.1
YCG-20	38°28′40″N, 93°55′21″E	Late Oligocene	Shang Ganchaigou Fm.	28	0.745 (1862)	5.035 (866)	1.221 (2100)	20.5	80.1	54.0 ± 2.9	14.25 ± 0.12	1.21
YCG-30	38°28′08″N, 93°55′13″E	Middle Miocene	Xia Youshashan Fm.	30	0.730 (1825)	4.845 (889)	0.912 (1673)	15.6	90.5	68.1 ± 3.8	14.41 ± 0.09	0.95
YCG-38	38°27′33″N, 93°55′2″E	Middle Miocene	Shang Youshashan Fm.	30	0.715 (1787)	4.339 (1076)	1.038 (2575)	18.2	0.9	55.8 ± 3.3	14.16 ± 0.11	1.1
B1-05[b]	37°46′2″N, 94°22′15″E	Middle Miocene	Shang Youshashan Fm.	30	0.956 (2390)	5.392 (895)	1.776 (2948)	23.2	0	57.5 ± 4.4	14.14 ± 0.10	0.97
X9-18[b]	37°56′18″N, 94°11′45″E	Middle Miocene	Xia Youshashan Fm.	28	0.820 (2051)	3.708 (634)	1.223 (2091)	18.6	0.5	47.3 ± 3.3	14.48 ± 0.11	1.16

Nc: number of apatite crystals analyzed; ρ_d: induced fission-track density calculated from muscovite external detectors used with SRM_{612} dosimeter; ρ_s: spontaneous fission-track density on the internal surfaces of apatite crystals analyzed; ρ_i: induced fission-track density on the muscovite external detector for crystals analyzed; N_d, N_s and N_i: total number of fission tracks counted in ρ_d, ρ_s and ρ_i, respectively; P(X^2): chi-squared probability that all single-crystal ages represent a single population of ages where degrees of freedom = Nc − 1; Apatite-$Zeta_{CN5}$ = 353.0 ± 10.

[a] Pooled AFT ages were used for samples with P (X^2) >5%, and mean AFT ages were used for samples with P (X^2) ≤5%.

[b] Borehole samples. The depths of Samples B1-05 and X9-18 are 1236 m and 814 m, respectively.

respectively (Fig. 3; Table 1). The two Early Cretaceous Samples LLH-16 and LLH-20 yield detrital AFT ages of 50.4 ± 2.9 Ma and 54.1 ± 2.9 Ma (Fig. 3; Table 1). The Cenozoic Samples YCG-03, YCG-09, YCG-20 and YCG-30 have detrital AFT ages at 51.3 ± 2.7 Ma, 53.8 ± 2.8 Ma, 54.0 ± 2.9 Ma and 68.1 ± 3.8 Ma, respectively, and these ages also pass X^2 test (Table 1). However, detrital AFT ages of the samples YCG-38, B1-05 and X9-18 (i.e. 55.8 ± 3.3 Ma, 57.5 ± 4.4 Ma and 47.3 ± 3.3 Ma, respectively) fail X^2 test (i.e. P (X^2) ≤ 5%), implying the presence of multiple age populations for each sample. Raw data of apatite fission track analysis are given in Tables A1–A2 (in the Supplementary data).

We modeled the time-temperature histories of those Mesozoic samples using a Monte-Carlo inversion algorithm of HeFTy (Ketcham, 2005). In addition to the AFT data, the ranges of possible thermal histories are constrained by sample depositional ages and a wide temperature window of burial temperatures (Fig. 3G). The good fit models of the Jurassic Samples DMG-13, DMG-31, JLS-07, JLS-11 and LLH-04 suggest that the onset of a cooling from ~120 °C was as early as the Late Cretaceous (>70 Ma), while the thermal models of the Late Jurassic Sample LLH-08 and Early Cretaceous Samples LLH-16 and LLH-20 indicate that ~120 °C cooling probably started at the early Paleogene.

Paleocurrent orientation data were collected from 4 locations on the Cenozoic YCG section (Fig. 4). The Xia Ganchaigou and Shang Ganchaigou Formations have overwhelmingly southwest-directed paleoflow (Fig. 4), while west-directed paleoflow orientations prevail during the Xia Youshashan Formation deposition time. The Shang Youshashan Formation has southwest- and west- directed paleoflow (Fig. 4).

5. Discussion

5.1. Temporal variations of Cenozoic sedimentary provenance for northern Qaidam basin

Fig. 6 shows the comparison between detrital AFT ages and depositional ages of the analyzed samples. The results indicate that the detrital AFT ages of the middle Eocene to late Oligocene samples (YCG-03, YCG-09 and YCG-20) range from 54 Ma to 51 Ma, while the detrital AFT ages of the Miocene samples (YCG-30, YCG-38, X9-18 and B1-05) from 68 Ma to 35 Ma (Fig. 6). Therefore, the detrital AFT ages of all the Cenozoic samples are older than their depositional ages (Fig. 6). The measured track-lengths show narrow length distributions (Figs. 4–5) and the track-length averages range from 13.38 ± 0.11 μm to 14.48 ± 0.11 μm (Table 1). Hence, we interpret that all the Cenozoic samples are unannealed, and the detrital apatite grains preserve cooling history of their parent-rocks. Table 2 displays Binomial (Brandon, 2002) peak-fitting results of the detrital AFT age data of the analyzed Cenozoic samples. All the ages fall into 2 age populations, i.e. Population 1 (P1, Eocene) and Population 2 (P2, Late Cretaceous to Paleocene) in Table 2.

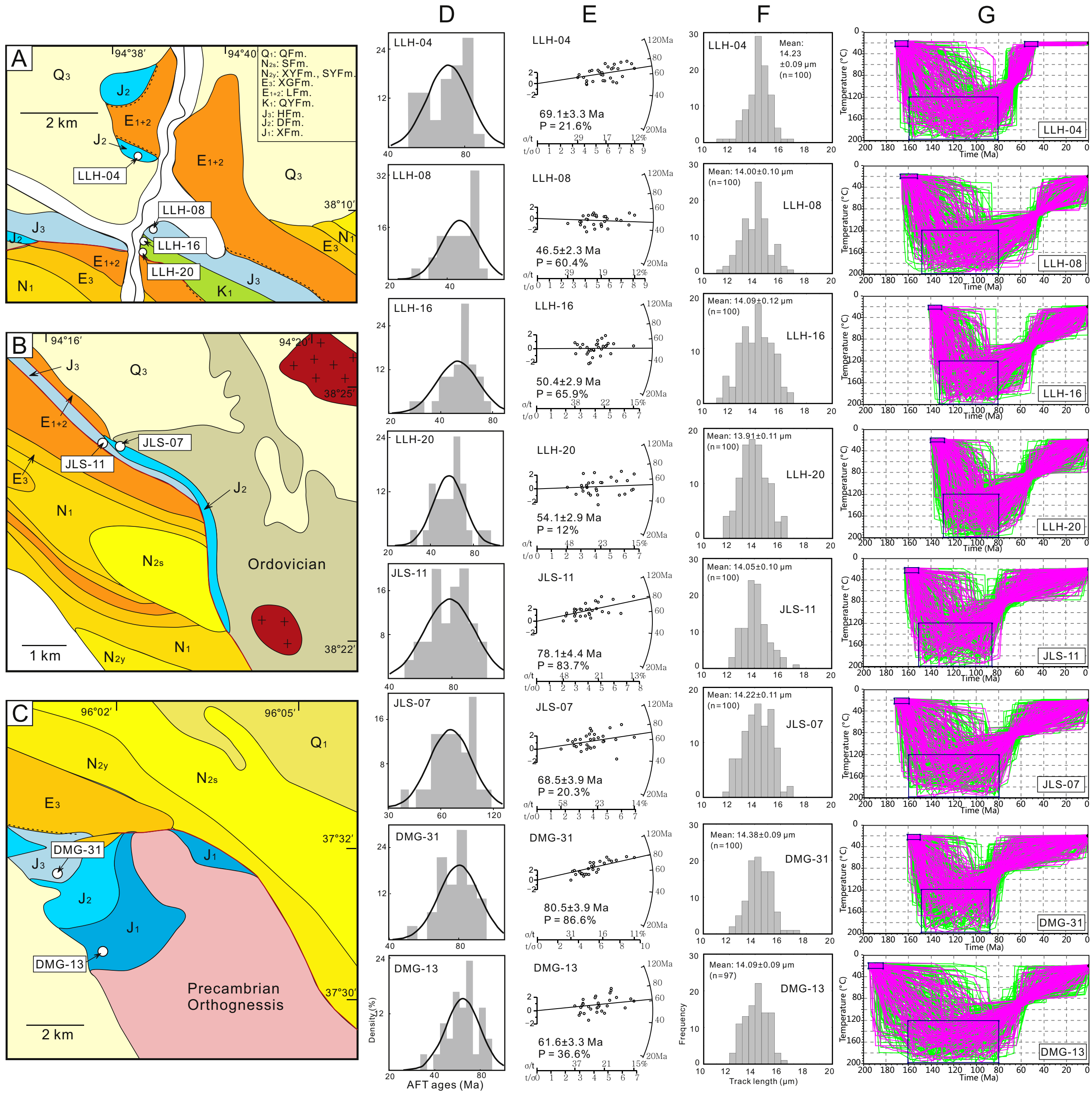

Fig. 3. Mesozoic sandstone sample locations (A–C) and detrital AFT analysis results (D–G). BINOMIAL software (Brandon, 2002) was used to illustrate probability plots of the detrital AFT ages. Radial plots (E) were obtained using RadialPlotter (Vermeesch, 2009). Models of time-temperature histories (G) were created using HeFTy (Ketcham, 2005). Pink and green lines on the time-temperature plots represent acceptable and good fit models for each sample. Red boxes represent geologic constraints. (For interpretation of the references to color in this figure legend, the reader is referred to the web version of this article.)

The published data of clast composition, heavy mineral, mineral chemistry, detrital mica $^{40}Ar/^{39}Ar$ age, detrital zircon U-Pb age and paleoflow direction, indicate that the North Qaidam and South Qilian terranes are major sources for the Cenozoic sedimentary rocks (Rieser et al., 2006; Zhuang et al., 2011; Jian et al., 2013a, 2013b). Therefore, the Cenozoic detrital AFT analysis results (Table 2; Figs. 4–5) reveal that the southern part of Qilian Mountains probably underwent widespread cooling (~120 °C–60 °C) during the Late Cretaceous to early Eocene. However, previous bedrock low-temperature thermochronology studies across the Qilian Mountains demonstrate extensive Neogene (20–10 Ma) exhumation and subordinate Early Cretaceous and late Paleogene exhumation (Fig. 1B). This means that the pre-Miocene exhumation in Qilian Mountains was likely underestimated. We infer that plenty of rocks had ever been exhumed during the Late Cretaceous to early Eocene in the southern part of Qilian Mountains and were subsequently eroded, and the materials were transported to the northern Qaidam basin.

Assuming sedimentary rocks in a basin are directly derived from a single adjacent source, the sedimentary rocks at the bottom of a stratigraphic succession document relatively early exhumation of parent-rocks and thus have older cooling ages, while sedimentary rocks at the top have relatively younger cooling ages (Bernet et al., 2009). However,

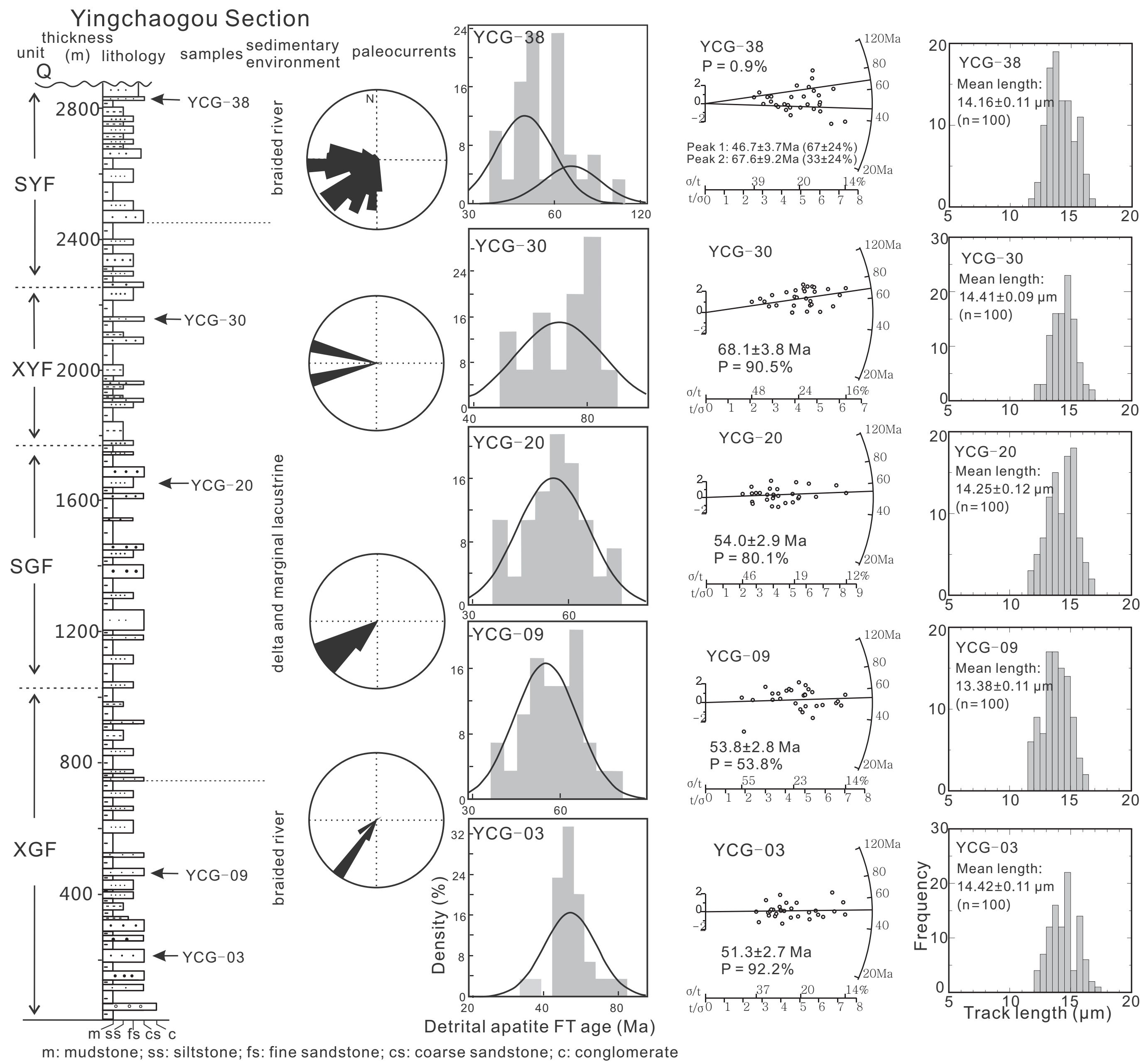

Fig. 4. Cenozoic YCG section, sedimentary environment interpretation (Guan and Jian, 2013), paleocurrent orientations and sandstone detrital AFT analysis results. BINOMIAL software (Brandon, 2002) was used to illustrate probability plots of the detrital AFT ages. Radial plots were obtained using RadialPlotter (Vermeesch, 2009). XGF: Xia Ganchaigou Formation, SGF: Shang Ganchaigou Formation, XYF: Xia Youshashan Formation, SYF: Shang Youshashan Formation.

detrital apatite grains from the Paleogene samples (YCG-03, YCG-09 and YCG-20) of the YCG section only have younger P1 fission track ages, whereas the relatively older P2 fission track ages can be largely detected in apatite grains from the Miocene samples (YCG-30 and YCG-38) (Fig. 4). This kind of detrital thermochronological pattern could be attributed to different source regions, i.e., an early source with younger cooling ages contributed detritus first and then other source regions with older cooling ages were involved in. This can be explained as follows. First, the paleocurrent data (Fig. 4) indicate dominantly southwest-directed paleoflow during the middle Eocene–Oligocene, while west-directed paleoflow orientations prevailed during the early Miocene and west- and southwest- directed paleoflow prevailed since the middle Miocene. Second, previous conglomerate clast composition, sandstone petrography and heavy mineral-based provenance analysis results suggest seemingly increasing contribution of metamorphic rocks to the depositional area since the early–middle Miocene (Zhuang et al., 2011; Jian et al., 2013a). The occurrence of two fission track age populations in the middle Miocene sedimentary rocks (Samples YCG-38, X9-18 and B1-05) reveals multiple source regions with different cooling histories contributing sediments at the same time.

5.2. Two stages of Late Cretaceous to early Eocene exhumation in northern Tibet

The detrital AFT ages of the Jurassic and Early Cretaceous samples range from 81 Ma to 46 Ma (Table 1), and are younger than their depositional ages (Fig. 6). This reveals that these Mesozoic sedimentary rocks were deeply (>6 km) buried and were subsequently exhumed, and have distinct deformation history from Cenozoic sedimentary rocks. The deep burial is also suggested by significant compaction and pressure-

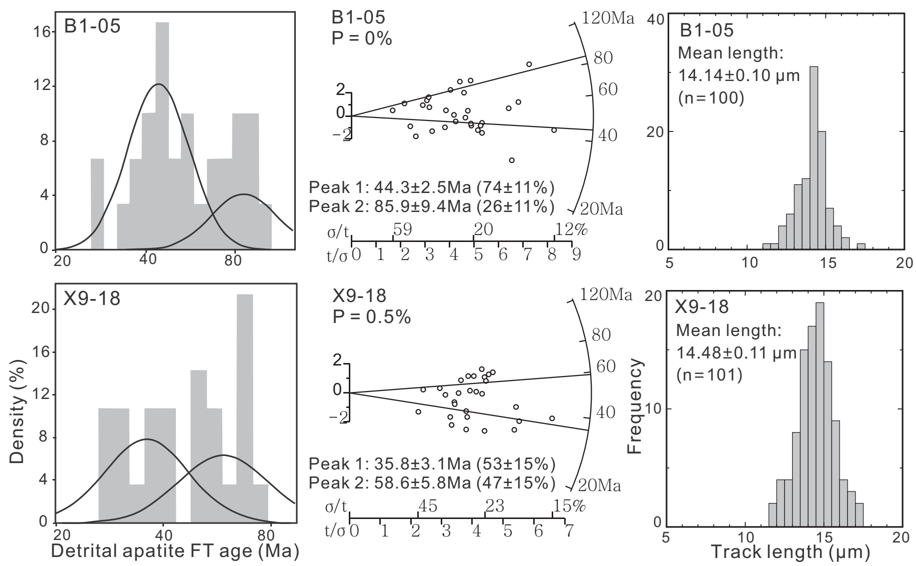

Fig. 5. Detrital AFT analysis results of two Cenozoic borehole samples. These two samples do not pass the X^2 test and thus have multiple AFT age populations calculated by BINOMIAL (Brandon, 2002). Radial plots were obtained using RadialPlotter (Vermeesch, 2009).

solution diagenesis of the Mesozoic sandstones (Jian et al., 2013b) and the thermal maturity (Ro = 1.0%) of the coal-bearing Lower and Middle Jurassic rocks (Ritts et al., 1999). Therefore, the detrital AFT analysis results in this study suggest that both the Mesozoic sedimentary succession in northern Qaidam basin and the southern part of Qilian Mountains experienced exhumation during the Late Cretaceous to early Eocene. Numerous Late Cretaceous to early Eocene cooling ages have also been reported by previous detrital thermochronological studies on Cenozoic sedimentary rocks from western Qaidam basin (Wang et al., 2015), southern Tarim basin (Yin et al., 2002), Subei basin (Lin et al., 2015), Jiuxi basin (W. Wang et al., 2016) and Guide-Xining basins (X. Wang et al., 2016) and thermochronological studies on the exposed bedrock and faults of the East Kunlun and Qinling Mountains (Fig. 1B). Thus, the Late Cretaceous to early Eocene exhumation was a regional rather than a local event in northern Tibet.

In general, upper sedimentary rocks present older cooling ages than lower sedimentary rocks in an exhumation event for deep-buried

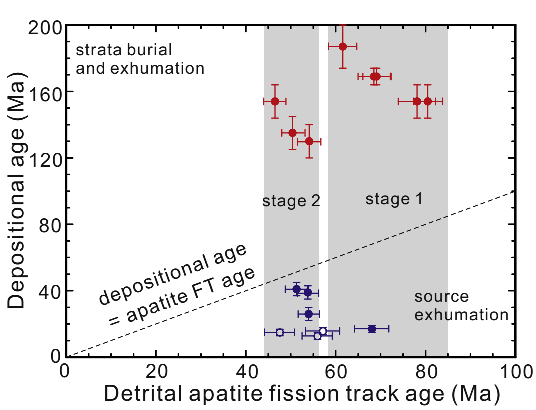

Fig. 6. Detrital AFT ages (Table 1) versus depositional ages of all the analyzed samples. The detrital AFT ages of Mesozoic samples (red symbols) are younger than their depositional ages, suggesting deep burial and subsequent exhumation of the rocks, whereas the detrital AFT ages of analyzed Cenozoic samples (blue symbols) are older than their depositional ages and thus represent source terrane exhumation ages. Depositional ages were estimated based on stratigraphic correlation and previous magnetostratigraphic studies on the typical sections (Fang et al., 2007; Lu and Xiong, 2009; Chang et al., 2015; Ji et al., 2017) in the Qaidam basin. Note that detrital AFT ages of Samples YCG-38, B1-05 and X9-18 (circle symbols) fail X^2 test. (For interpretation of the references to color in this figure legend, the reader is referred to the web version of this article.)

sedimentary strata. The Upper Jurassic Samples JLS-11 and DMG-31 have relatively consistent detrital AFT ages, i.e., 78.1 ± 4.4 Ma and 80.5 ± 3.9 Ma, respectively. These ages are older than the detrital AFT ages of the Middle and Lower Jurassic Samples JLS-07 (68.5 ± 3.9 Ma) and DMG-13 (61.6 ± 3.3 Ma) from the two sections, implying that these Jurassic samples experienced one-stage of exhumation during ca. 80–61 Ma. However, the Upper Jurassic and Lower Cretaceous Samples LLH-08, LLH-16 and LLH-20 from the LLH section (Fig. 3) have younger detrital AFT ages (46.5 ± 2.3 Ma, 50.4 ± 2.9 Ma and 54.1 ± 2.9 Ma, respectively) than the Middle Jurassic Sample LLH-04 (69.1 ± 3.3 Ma), revealing that the Mesozoic LLH section probably experienced two stages of exhumation events. The two-stage exhumation is also reflected by the HeFTy thermal models (Fig. 3). Given the similar exhumation ages between the Middle Jurassic LLH and JLS sections, the exhumation of the Middle Jurassic LLH section is related to the same phase of exhumation that is identified in the JLS and DMG sections. Collectively, the Late Cretaceous to early Eocene exhumation in all the analyzed Mesozoic rocks at least consists of two stages, ca. 80–61 Ma and ca. 54–47 Ma (Fig. 6).

As mentioned above, the detrital AFT ages of Cenozoic rocks can also be separated into two age populations, with the peak age ranges of 86–59 Ma and 54–36 Ma (Figs. 4–5, Table 2), implying two stages of cooling and uplift of sedimentary sources during the Late Cretaceous to Eocene. Furthermore, lag-time concept is employed to determine exhumation rates in source terranes for the Cenozoic samples. The lag-time represents the difference between the time cooling minerals pass through a closure isotherm in the source region and deposition time in the adjacent basin (Garver et al., 1999; Bernet et al., 2006). To evaluate the source exhumation rate, this concept assumes that detritus transport time is negligible at geological time scales (Brandon and Vance, 1992). Thus, the lag-time is calculated as the peak cooling age minus the depositional age (Garver et al., 1999; Bernet et al., 2006). A shortening trend of lag-time indicates accelerating exhumation over time, while an increase in lag-time reveals a decrease in exhumation rates, and constant lag-times reflect continuous exhumation at a certain rate and long-term balance between convergence mass influx and exhumation outflux (Bernet and Garver, 2005). The detrital AFT peak ages for those Paleogene samples (i.e. YCG-03, YCG-09 and YCG-20) of the YCG section are approximately constant (with errors) and the lag time correspondingly increases continuously up-section (Table 2, Fig. 7). This situation is regarded as a static peak (Brandon and Vance, 1992). Bernet et al. (2006) states that a static peak could be either

Table 2
Binomial peak-fitting results of detrital apatite fission track data of Cenozoic sandstone samples.

Sample	Depositional age	Population 1				Population 2				$P(X^2)$ %
		Peak (Ma)	CI (95%)	CI (68%)	Frac (%)	Peak (Ma)	CI (95%)	CI (68%)	Frac (%)	
B1-05	Middle Miocene (14 ± 2 Ma)	44.3	−4.7/+5.2	−2.5/+2.6	73.6	85.7	−16.9/+21.0	−9.1/+10.1	26.4	0.0
X9-18	Middle Miocene (16 ± 2 Ma)	35.9	−5.5/+6.5	−2.9/+3.2	53.8	58.7	−10.4/+12.7	−5.6/+6.1	46.2	0.5
YCG-38	Middle Miocene (13 ± 2 Ma)	47.1	−6.6/+7.7	−3.5/+3.8	70.3	69	−16.7/+22.0	−9.1/+10.5	29.7	0.9
YCG-30	Middle Miocene (17 ± 2 Ma)	–	–		–	68.1	−6.4/+7.0	−3.3/+3.5	100	90.5
YCG-20	Late Oligocene (26 ± 4 Ma)	54	−5.0/+5.5	−2.6/+2.7	100	–	–		–	80.1
YCG-09	Late Eocene (39 ± 4 Ma)	53.8	−4.8/+5.2	−2.5/+2.6	100	–	–		–	53.8
YCG-03	Late Eocene (41 ± 4 Ma)	51.3	−4.5/+5.0	−2.4/+2.5	100	–	–		–	92.2

Note that the detrital AFT ages for the analyzed Cenozoic samples are older than the corresponding depositional ages, implying these ages represent cooling ages of source parent-rocks. BINOMIAL software (Brandon, 2002) was employed to obtain the peak ages.

(A) attributed to a source terrane that experienced a rapid but short-lived cooling event, (B) due to recycling of a sedimentary source, in particular if the peak age is relatively old and predates orogenesis or (C) derived from thick and non-reset volcanic rocks. The peak ages are relatively young (ca. 54–51 Ma) and early Eocene volcanic activity was rare within and along the Qilian Mountains (e.g., Ding et al., 2003; Taylor and Yin, 2009; Xia et al., 2011). Therefore, we advocate that the North Qaidam and South Qilian terranes, as the main sediment sources, likely experienced fast exhumation during the early Eocene and was then subsequently exhumed slowly and eroded into the Qaidam basin until at least the early Miocene.

5.3. Tectonic evolution of the northern Tibet since the Late Cretaceous

Most studies agree that the central Tibetan crust was thickened substantially prior to the India-Eurasia collision (e.g., Kapp et al., 2005, 2007; Volkmer et al., 2007). Thermochronological evidence infers rapid to moderate cooling and substantial surface elevation gain in central Tibet during the Cretaceous to Eocene (Wang et al., 2008; Rohrmann et al., 2012), and paleoelevation estimates suggest that most areas of Lhasa and Qiangtang terranes were likely elevated to near-modern altitudes by the late Paleogene (e.g., Rowley and Currie, 2006; Polissar et al., 2009; Xu et al., 2013; Ding et al., 2014). If the Cretaceous Eurasian plate had an Andean-type margin in the south, the thickened lithosphere of central Tibet was attributed to the northward subduction of the Neo-Tethys oceanic plate (Ding et al., 2014; Lippert et al., 2014; Staisch et al., 2016). Our new detrital AFT analysis results

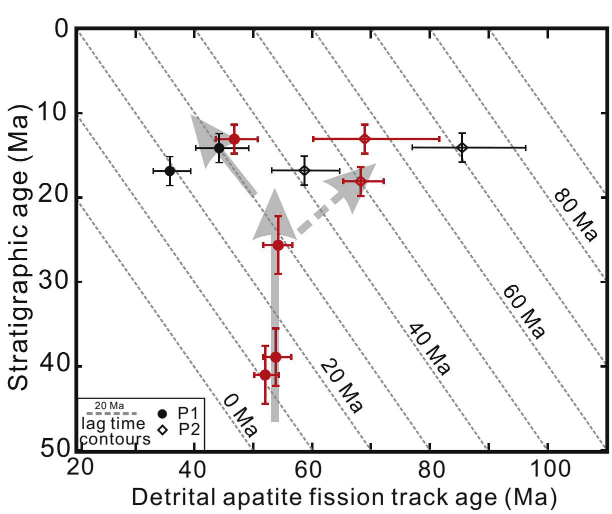

Fig. 7. Lag-time analysis of detrital AFT peak ages for the Cenozoic samples. The YCG section and Maxian samples are shown as red and black symbols, respectively. Gray solid lines with arrows show variation trends of P1 ages, while the dashed gray arrow indicates the occurrence of P2 ages and hence provenance changes. The uncertainties for the peak ages are given at 68% confidence intervals. (For interpretation of the references to color in this figure legend, the reader is referred to the web version of this article.)

indicate widespread Late Cretaceous–middle Paleocene (86–59 Ma) exhumation in northern Tibet. This means that the extent of the pre-collisional deformation region might be much larger than previously known (Fig. 8A). In this case, Late Cretaceous–middle Paleocene subduction of the Neo-Tethys lithosphere even influenced the tectonics of current north margin of the Tibet plateau. This might make us to reconsider the nature of the subduction zone in the south margin of the Eurasian plate before the India-Eurasia collision. Although the elevation and the amount of crustal thickening of northern Tibet prior to the collision remain less well known, the northern Tibet was likely involved in pre-collisional development of the whole plateau.

The published low-temperature thermochronological data in the Qilian Mountains demonstrate widespread deformation during the Neogene (20–10 Ma) (George et al., 2001; Zheng et al., 2010; Lease et al., 2011; Duvall et al., 2013), whereas the Eocene cooling signals are minor (Fig. 1B). Conversely, The East Kunlun shows abundant Eocene cooling ages (Fig. 1B). This is seemingly consistent with the model of northward propagating deformation within the northern Tibet, which predicts the Qilian Mountains experienced much later deformation and uplift than the East Kunlun (Wang et al., 2008). However, our new detrital AFT results, combined with previous thermochronological, stratigraphic and basin structural analysis results (e.g., Yin et al., 2002; Clark et al., 2010; Duvall et al., 2011; Zhuang et al., 2011; F. Wang et al., 2016), favor synchronous distributed deformation and crustal shortening throughout the northern plateau near the onset of the India-Eurasia collision (Clark, 2012). Regardless of whether high topography was or was not built simultaneously as a result of this deformation event, more and more evidence suggests that the northern boundary of the plateau was established once the India-Eurasia collision commenced at ca. 55–50 Ma. The far-field stress resulted in accelerated exhumation, rapid erosion and deposition (Fig. 8B), as well as the formation of Cenozoic basins in northern Tibet (Yin et al., 2008a, 2008b; Clark et al., 2010; Zhuang et al., 2011; Guan and Jian, 2013).

It is worth noting that the middle Miocene samples don't have Oligocene to early Miocene cooling ages (Figs. 3–5), implying quiescence in exhumation of the southern Qilian Mountains during the Oligocene to early Miocene. Lag-time analysis of those Paleogene samples indicates decreasing exhumation rates of the source regions at least from late Eocene to late Oligocene (Fig. 7). Furthermore, the low-temperature thermochronology results of the thrust faulting-related bedrocks also support Oligocene to early Miocene quiescence in range-bounding thrust faulting activities in the Qilian Mountains (Zhuang et al., 2018). Collectively, the Qilian Mountains were likely in relatively quiescent tectonic settings during the Oligocene to early Miocene. This inference is consistent with balanced cross-section restoration studies which show the minima crustal thickening during that time (Zhou et al., 2006). The weak exhumation and deformation is also reflected by the sedimentation in Qaidam basin, where the Shang Ganchaigou and Xia Youshashan Formations mainly consist of fine-grained fluvio-lacustrine sedimentary rocks under low-gradient depositional systems (Zhuang et al., 2011; Guan and Jian, 2013). We favor that this relatively quiescent tectonic setting of the Qilian Mountains was probably related

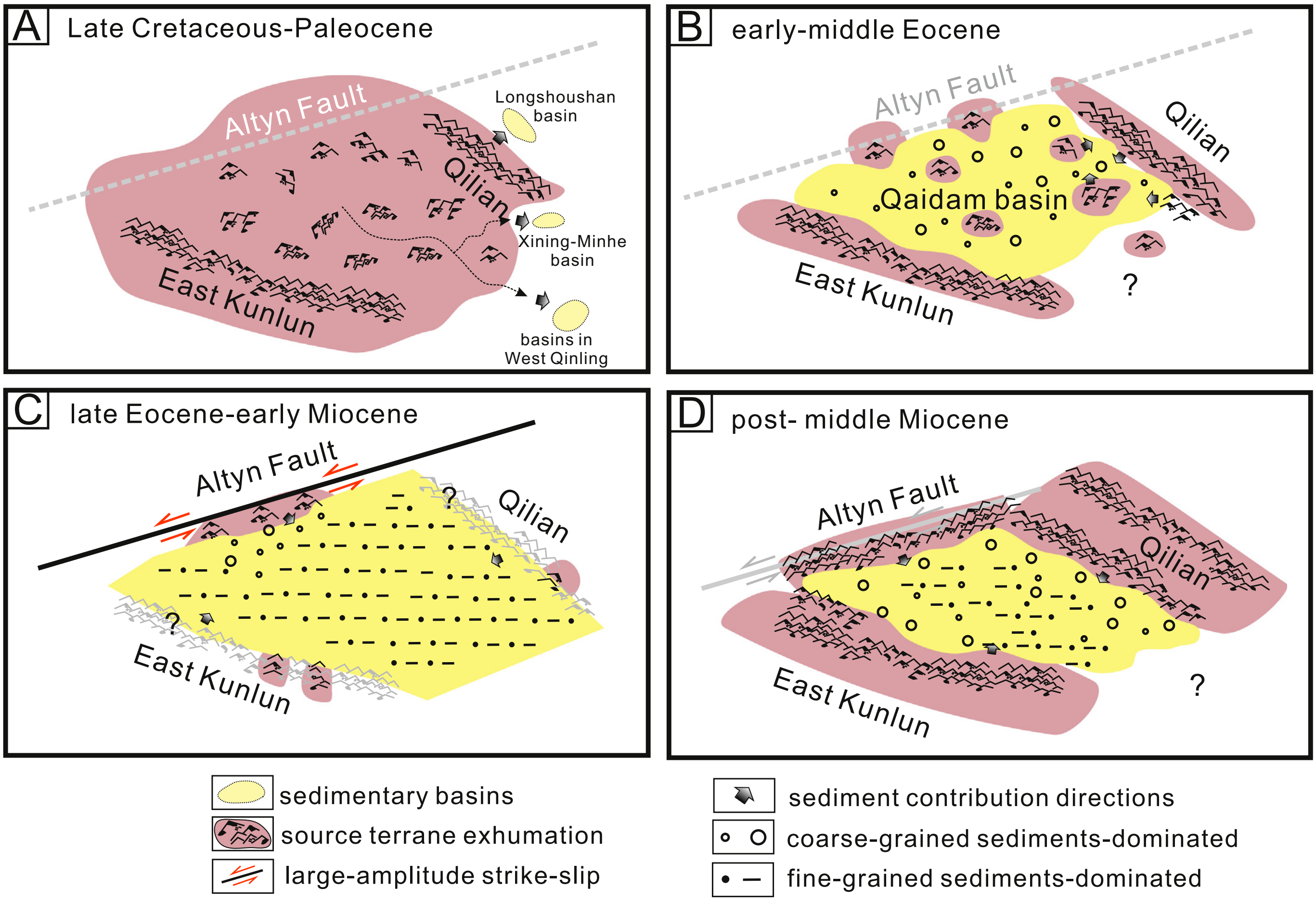

Fig. 8. Tectono-sedimentary evolution of the Qaidam basin and the surrounding regions. (A) Widespread exhumation and deformation in both the basin and surrounding orogenic belt regions during the Late Cretaceous to Paleocene and limited depocenters (e.g., Xining-Minhe and Longshoushan basins (Li et al., 2006)) in northeastern Tibet. (B) Rapid exhumation and uplift of the orogenic belts and pre-Cenozoic basin basements shortly after the India-Eurasia collision and formation of the Cenozoic Qaidam basin. Sediments in the basin during that time were dominated by coarse-grained sediments with nearby sources. (C) Large-amplitude lateral strike-slip of the Altyn Tagh fault was accommodated out of Tibet plateau during the late Eocene to early Miocene and resulted in relatively quiescent tectonic settings and little crustal thickening in Qilian Mountains and dominant fine-grained sediments in Qaidam basin. (D) Extensive deformation and rapid uplift of the major orogenic belts since the middle Miocene have resulted in the current tectonic framework in northern Tibet.

to large-amplitude lateral offset and extrusion along the sinistral strike-slip Altyn Tagh Fault (Fig. 8C) before the end of early Miocene time (Yue and Liou, 1999; Yue et al., 2003; Lu et al., 2016). The slip motion of the Altyn Tagh Fault was accommodated out of the plateau, rather than within the plateau during ca. 36–18 Ma (Yue and Liou, 1999; Yue et al., 2003), resulting in very weak and low-rate crustal thickening in the Qilian Mountains (Bovet et al., 2009; Lease et al., 2012; Zhang et al., 2014).

Sediment provenance variations and dramatic changes of detrital AFT lag-time (Fig. 7) at ca. 17 Ma were likely due to rapid uplift and intensive deformation of the North Qaidam and South Qilian terranes since the middle Miocene. This is consistent with results of Zhuang et al. (2018), which show that Neogene exhumation started in the south of Qilian Mountains prior to 18–16 Ma. This uplift event is also supported by the high-gradient depositional systems in the northern margin of the Qaidam basin (Zhuang et al., 2011; Guan and Jian, 2013) and relatively higher sediment accumulation rates since the middle–late Miocene (Fang et al., 2007; Lu and Xiong, 2009; Ji et al., 2017). Although the detrital AFT presented in this study do not contain middle Miocene or younger cooling ages, numerous published fission-track analysis and (U-Th)/He thermochronological data indicate a fast exhumation event during the middle–late Miocene throughout the Qilian Mountains (Fig. 1B; George et al., 2001; Zheng et al., 2010; Lease et al., 2011; Lu et al., 2012; Duvall et al., 2013; Zhuang et al., 2018). Combined with the Late Cenozoic tectonic history of the other adjacent orogenic belts, e.g. East Kunlun, Altun Mountains and West Qinling (e.g., Duvall et al., 2013; Chang et al., 2015; Lu et al., 2016), we favor that the rapid uplift of Qilian Mountains was a part of a tectonic reorganization in northern Tibet during the middle Miocene (Fig. 8D). Given the coevality of increasing Pacific-Asia plate convergence rates and this tectonic reorganization, Zhuang et al. (2018) argued that the increasing constrictive environment of the eastern plate boundary changed the behavior of the Altyn Tagh Fault, causing it to change from feeding slip into structures out of the plateau to feeding slip into structures at plateau margins. This widely distributed deformation resulted in substantial crustal shortening in these orogenic belts and thus led to near-modern elevations and the current tectonic framework in northern Tibet (Polissar et al., 2009; Lease et al., 2012; Zhang et al., 2014; Sun et al., 2015; Miao et al., 2016).

6. Conclusions

AFT-based detrital thermochronology of Jurassic, Early Cretaceous and Cenozoic sandstone samples from the northern Qaidam basin yields the following conclusions concerning the tectonic evolution and deformation history of northern Tibet:

1) The northern Tibet regionally underwent Late Cretaceous to middle Paleocene exhumation and early Eocene rapid but short-lived exhumation in the early deformation history. The former exhumation suggests that the extent of the pre-collisional (India-Eurasia) deformation region in the plateau might be much larger than previously known, which was probably attributed to the northward subduction of the Neo-Tethys oceanic plate. The latter exhumation and corresponding mountain-building and Cenozoic basin formation were likely a far-field response to the collision between Indian and Eurasian plates, signifying synchronous distributed deformation and crustal shortening throughout the northern plateau near the onset of the collision.
2) The detrital AFT ages and lag-time analysis results of the Cenozoic samples suggest relatively a quiescent tectonic setting and decreasing exhumation rates in Qilian Mountains during the late Eocene to early Miocene. This was probably related to large-amplitude lateral strike-slip movement of the Altyn Tagh Fault before the end of early Miocene, which was accommodated out of the plateau and resulted in little crustal shortening in Qilian Mountains.
3) The differences among the detrital AFT ages of the analyzed Cenozoic samples reveal sedimentary provenance changes at ca. 17 Ma, which was probably associated with the rapid uplift and intensive deformation of the Qilian Mountains since the middle Miocene.

Acknowledgments

This research was supported by Natural Science Foundation of Fujian Province (No. 2017J05067), Xiamen University Fundamental Research Funds for the Central Universities (No. 20720160114), Internal program at the State Key Laboratory of Marine Environmental Science (No. MELRI1703), Open Project at the State Key Laboratory of Marine Geology (No. MGK1706) and National Basic Research Program of China (No. 2012CB214801). We thank Ruijuan Liu, Shibiao Deng and Xiaoqin Xie for assistance in the field, Jianzhang Pang for his help in apatite fission track analysis and constructive discussions. We are grateful to Dr. Will Jackson for their efforts in improving the English language of the original manuscript. Two reviewers Gilby Jepson and Delores M. Robinson provided thoughtful reviews that improved this manuscript.

Appendix A. Supplementary data

Supplementary data to this article can be found online at https://doi.org/10.1016/j.gr.2018.04.007.

References

Bally, A.W., Chou, I.-M., Clayton, R., Eugster, H.P., Kidwell, S., Meckel, L.D., Ryder, R.T., Watts, A.B., Wilson, A.A., 1986. Notes on sedimentary basins in China—report of the American sedimentary basins delegation to the People's Republic of China. U.S. Geological Survey Open-File Report 86–327, 108.

Bernet, M., Garver, J.I., 2005. Fission-track analysis of detrital zircon. Reviews in Mineralogy and Geochemistry 58, 205–237.

Bernet, M., Beek, P., Pik, R., Huyghe, P., Mugnierz, J.L., Labrinz, E., Szulc, A., 2006. Miocene to Recent exhumation of the central Himalaya determined from combined detrital zircon fission-track and U/Pb analysis of Siwalik sediments, western Nepal. Basin Research 18, 393–412.

Bernet, M., Brandon, M., Garver, J., Balestieri, M.L., Ventura, B., Zattin, M., 2009. Exhuming the Alps through time: clues from detrital zircon fission track thermochronology. Basin Research 21, 781–798.

Bovet, P.M., Ritts, B.D., Gehrels, G., Abbink, A.O., Darby, B., Hourigan, J., 2009. Evidence of Miocene crustal shortening in the North Qilian Shan from Cenozoic stratigraphy of the western Hexi Corridor, Gansu Province, China. American Journal of Science 309, 290–329.

Brandon, M.T., 2002. Decomposition of mixed grain age distributions using Binomfit. On Track. 24, pp. 13–18.

Brandon, M.T., Vance, J.A., 1992. New statistical methods for analysis of fission track grain-age distributions with applications to detrital zircon ages from the Olympic subduction complex, western Washington State. American Journal of Science 292, 565–636.

Chang, H., Li, L., Qiang, X., Garzione, C.N., Pullen, A., An, Z., 2015. Magnetostratigraphy of Cenozoic deposits in the western Qaidam Basin and its implication for the surface uplift of the northeastern margin of the Tibetan Plateau. Earth Planet. Sci. Lett. 430, 271–283.

Cheng, F., Jolivet, M., Hallot, E., Zhang, D., Zhang, C., Guo, Z., 2017. Tectono-magmatic rejuvenation of the Qaidam craton, northern Tibet. Gondwana Res. 49, 248–263.

Clark, M.K., 2012. Continental collision slowing due to viscous mantle lithosphere rather than topography. Nature 483 (7387), 74–77.

Clark, M.K., Farley, K.A., Zheng, D., Wang, Z., Duvall, A.R., 2010. Early Cenozoic faulting of the northern Tibetan Plateau margin from apatite (U–Th)/He ages. Earth and Planetary Science Letters 296, 78–88.

Dai, J., Wang, C., Hourigan, J., Santosh, M., 2013. Multi-stage tectono-magmatic events of the eastern Kunlun Range, northern Tibet: insights from U–Pb geochronology and (U–Th)/He thermochronology. Tectonophysics 599, 97–106.

Ding, L., Kapp, P., Zhong, D., Deng, W., 2003. Cenozoic volcanism in Tibet: evidence for a transition from oceanic to continental subduction. Journal of Petrology 44, 1833–1865.

Ding, L., Xu, Q., Yue, Y., Wang, H., Cai, F., Li, S., 2014. The Andean-type Gangdese Mountains: Paleoelevation record from the Paleocene–Eocene Linzhou Basin. Earth and Planetary Science Letters 392, 250–264.

Dupont-Nivet, G., Horton, B.K., Butler, R.F., Wang, J., Zhou, J., Waanders, G.L., 2004. Paleogene clockwise tectonic rotation of the Xining-Lanzhou region, northeastern Tibetan Plateau. Journal of Geophysical Research - Solid Earth 109, B04401. https://doi.org/10.1029/2003JB002620.

Duvall, A.R., Clark, M.K., van der Pluijm, B.A., Li, C., 2011. Direct dating of Eocene reverse faulting in northeastern Tibet using Ar-dating of fault clays and low-temperature thermochronometry. Earth and Planetary Science Letters 304, 520–526.

Duvall, A.R., Clark, M.K., Kirby, E., Farley, K.A., Craddock, W.H., Li, C., Yuan, D.Y., 2013. Low-temperature thermochronometry along the Kunlun and Haiyuan Faults, NE Tibetan Plateau: evidence for kinematic change during late-stage orogenesis. Tectonics 32, 1190–1211.

England, P., Houseman, G., 1986. Finite strain calculations of continental deformation: 2. Comparison with the India-Asia collision zone. Journal of Geophysical Research - Solid Earth 91 (B3):3664–3676. https://doi.org/10.1029/JB091iB03p03664.

England, P., McKenzie, D., 1982. A thin viscous sheet model for continental deformation. Geophysical Journal International 70, 295–321.

Fang, X., Zhang, W., Meng, Q., Gao, J., Wang, X., King, J., Song, C., Dai, S., Miao, Y., 2007. High-resolution magnetostratigraphy of the Neogene Huaitoutala section in the eastern Qaidam Basin on the NE Tibetan Plateau, Qinghai Province, China and its implication on tectonic uplift of the NE Tibetan Plateau. Earth and Planetary Science Letters 258, 293–306.

Garver, J.I., Brandon, M.T., Roden-Tice, M.K., Kamp, P.J.J., 1999. Exhumation history of orogenic highlands determined by detrital fission track thermochronology. In: Ring, U., Brandon, M.T., Lister, G., Willett, S.D. (Eds.), Exhumation Processes: Normal faulting, Ductile Flow, and Erosion. Geological Society, London, Special Publications 154, pp. 283–304.

Gehrels, G., Yin, A., Wang, X., 2003. Detrital-zircon geochronology of the northeastern Tibetan Plateau. Geological Society of America Bulletin 115, 881–896.

George, A.D., Marshallsea, S.J., Wyrwoll, K.H., Jie, C., Yanchou, L., 2001. Miocene cooling in the northern Qilian Shan, northeastern margin of the Tibetan Plateau, revealed by apatite fission-track and vitrinite-reflectance analysis. Geology 29, 939–942.

Gleadow, A.J.W., Duddy, I.R., 1981. A natural long-term annealing experiment for apatite. Nuclear Tracks 5, 169–174.

Guan, P., Jian, X., 2013. The Cenozoic sedimentary record in Qaidam basin and its implications for tectonic evolution of the northern Tibetan plateau. Acta Sedimentologica Sinica 31, 824–833 (In Chinese with English Abstract).

Harrison, T.M., Copeland, P., Kidd, W.S.F., Yin, A., 1992. Raising Tibet. Science 255, 1663–1670.

Huang, H., Niu, Y., Nowell, G., Zhao, Z., Yu, X., Zhu, D.C., Mo, X., Ding, S., 2014. Geochemical constraints on the petrogenesis of granitoids in the East Kunlun Orogenic belt, northern Tibetan Plateau: implications for continental crust growth through syn-collisional felsic magmatism. Chemical Geology 370, 1–18.

Hurford, A.J., Green, P.F., 1983. The zeta age calibration of fission-track dating. Chemical Geology 1, 285–317.

Ji, J., Zhang, K., Clift, P.D., Zhuang, G., Song, B., Ke, X., Xu, Y., 2017. High-resolution magnetostratigraphic study of the Paleogene-Neogene strata in the northern Qaidam Basin: implications for the growth of the northeastern Tibetan Plateau. Gondwana Research 46, 141–155.

Jian, X., Guan, P., Zhang, D.-W., Zhang, W., Feng, F., Liu, R.-J., Lin, S.-D., 2013a. Provenance of Tertiary sandstone in the northern Qaidam basin, northeastern Tibetan Plateau: integration of framework petrography, heavy mineral analysis and mineral chemistry. Sedimentary Geology 290, 109–125.

Jian, X., Guan, P., Zhang, W., Feng, F., 2013b. Geochemistry of Mesozoic and Cenozoic sediments in the northern Qaidam basin, northeastern Tibetan Plateau: implications for provenance and weathering. Chemical Geology 360, 74–88.

Jian, X., Guan, P., Fu, S.-T., Zhang, D.-W., Zhang, W., Zhang, Y.-S., 2014. Miocene sedimentary environment and climate change in the northwestern Qaidam basin, northeastern Tibetan Plateau: facies, biomarker and stable isotopic evidences. Palaeogeography, Palaeoclimatology, Palaeoecology 414, 320–331.

Jolivet, M., Brunel, M., Seward, D., Xu, Z., Yang, J., Roger, F., Tapponnier, P., Malavieille, J., Arnaud, N., Wu, C., 2001. Mesozoic and Cenozoic tectonics of the northern edge of the Tibetan plateau: fission-track constraints. Tectonophysics 343, 111–134.

Kapp, P., Yin, A., Harrison, T.M., Ding, L., 2005. Cretaceous–Tertiary shortening, basin development, and volcanism in central Tibet. Geological Society of America Bulletin 117, 865–878.

Kapp, P., DeCelles, P.G., Gehrels, G.E., Heizler, M., Ding, L., 2007. Geological records of the Lhasa-Qiangtang and Indo-Asian collisions in the Nima area of central Tibet. Geological Society of America Bulletin 119, 917–933.

Ketcham, R.A., 2005. Forward and inverse modeling of low-temperature thermochronometry data. Reviews in Mineralogy and Geochemistry 58, 275–314.

Lease, R.O., Burbank, D.W., Clark, M.K., Farley, K.A., Zheng, D., Zhang, H., 2011. Middle Miocene reorganization of deformation along the northeastern Tibetan Plateau. Geology 39, 359–362.

Lease, R.O., Burbank, D.W., Zhang, H., Liu, J., Yuan, D., 2012. Cenozoic shortening budget for the northeastern edge of the Tibetan Plateau: is lower crustal flow necessary? Tectonics 31, TC3011.

Li, X., Chen, Q., Wei, W., Zuo, G., Wang, Q., Meng, Z., 2006. Distribution of Cretaceous proto-basin and basin-mountain frame work in Iner Mongolia-Gansu-Qinghai Area. Journal of Earth Sciences and Environment 28, 24–30 (In Chinese with English Abstract).

Li, W., Neubauer, F., Liu, Y., Genser, J., Ren, S., Han, G., Liang, C., 2013. Paleozoic evolution of the Qimantagh magmatic arcs, eastern Kunlun Mountains: constraints from zircon dating of granitoids and modern river sands. Journal of Asian Earth Sciences 77, 183–202.

Lin, X., Zheng, D., Sun, J., Windley, B.F., Tian, Z., Gong, Z., Jia, Y., 2015. Detrital apatite fission track evidence for provenance change in the Subei Basin and implications for the tectonic uplift of the Danghe Nan Shan (NW China) since the mid-Miocene. Journal of Asian Earth Sciences 111, 302–311.

Lippert, P.C., van Hinsbergen, D.J.J., Dupont-Nivet, G., 2014. Early Cretaceous to present latitude of the central proto-Tibetan Plateau: a paleomagnetic synthesis with implications for Cenozoic tectonics, paleogeography, and climate of Asia. Geological Society of America Special Papers 507, 1–21.

Liu, D., Li, H., Sun, Z., Pan, J., Wang, M., Wang, H., 2017. AFT dating constrains the Cenozoic uplift of the Qimen Tagh Mountains, northeast Tibetan Plateau, comparison with LA-ICPMS zircon U–Pb ages. Gondwana Research 41, 438–450.

Lu, H., Xiong, S., 2009. Magnetostratigraphy of the Dahonggou section, northern Qaidam Basin and its bearing on Cenozoic tectonic evolution of the Qilian Shan and Altyn Tagh Fault. Earth and Planetary Science Letters 288, 539–550.

Lu, H., Wang, E., Shi, X., Meng, K., 2012. Cenozoic tectonic evolution of the Elashan range and its surroundings, northern Tibetan Plateau as constrained by paleomagnetism and apatite fission track analyses. Tectonophysics 580, 150–161.

Lu, H., Fu, B., Shi, P., Ma, Y., Li, H., 2016. Constraints on the uplift mechanism of northern Tibet. Earth and Planetary Science Letters 453, 108–118.

Miao, Y., Wu, F., Chang, H., Fang, X., Deng, T., Sun, J., Jin, C., 2016. A Late-Eocene palynological record from the Hoh Xil Basin, northern Tibetan Plateau, and its implications for stratigraphic age, paleoclimate and paleoelevation. Gondwana Research 31, 241–252.

Molnar, P., England, P., Joseph, M., 1993. Mantle dynamics, uplift of the Tibetan plateau and the Indian monsoon. Reviews of Geophysics 31, 357–396.

Murphy, M.A., Yin, A., Harrison, T.M., Dürr, S.B., Chen, Z., Ryerson, F.J., Kidd, W.S.F., Wang, X., Zhou, X., 1997. Did the Indo-Asian collision alone create the Tibetan plateau? Geology 25, 719–722.

Najman, Y., Appel, E., Boudagher-Fadel, M., Bown, P., Carter, A., Garzanti, E., Godin, L., Han, J., Liebke, U., Oliver, G., Parrish, R., Vezzoli, G., 2010. Timing of India-Asia collision: geological, biostratigraphic, and palaeomagnetic constraints. Journal of Geophysical Research - Solid Earth 115, B12416. https://doi.org/10.1029/2010JB007673.

Polissar, P.J., Freeman, K.H., Rowley, D.B., McInerney, F.A., Currie, B.S., 2009. Paleoaltimetry of the Tibetan Plateau from D/H ratios of lipid biomarkers. Earth and Planetary Science Letters 287, 64–76.

Qi, B., Hu, D., Yang, X., Zhang, Y., Tan, C., Zhang, P., Feng, C., 2016. Apatite fission track evidence for the Cretaceous–Cenozoic cooling history of the Qilian Shan (NW China) and for stepwise northeastward growth of the northeastern Tibetan Plateau since early Eocene. Journal of Asian Earth Sciences 124, 28–41.

Rieser, A.B., Liu, Y., Genser, J., Neubauer, F., Handler, R., Ge, X.-H., 2006. Uniform Permian $^{40}Ar/^{39}Ar$ detrital mica ages in the eastern Qaidam Basin (NW China): where is the source? Terra Nova 18, 79–87.

Ritts, B.D., Biffi, U., 2001. Mesozoic northeast Qaidam basin: response to contractional reactivation of the Qilian Shan, and implications for the extent of Mesozoic intracontinental deformation in central Asia. Memoir - Geological Society of America 194, 293–316.

Ritts, B.D., Hanson, A.D., Zinniker, D., Moldowan, J.M., 1999. Lower–Middle Jurassic nonmarine source rocks and petroleum systems of the northern Qaidam basin, NW China. AAPG Bulletin 83, 1980–2005.

Rohrmann, A., Kapp, P., Carrapa, B., Reiners, P.W., Guynn, J., Ding, L., Heizler, M., 2012. Thermochronologic evidence for plateau formation in central Tibet by 45 Ma. Geology 40, 187–190.

Rowley, D.B., Currie, B.S., 2006. Palaeo-altimetry of the late Eocene to Miocene Lunpola basin, central Tibet. Nature 439, 677–681.

Ruddiman, W.F., Raymo, M.E., Prell, W.L., Kutzbach, J.E., 1997. The uplift-climate connection: a synthesis. In: Ruddiman, W.F. (Ed.), Tectonic Uplift and Climate Change. Plenum Press, New York, pp. 471–515.

Song, S., Niu, Y., Su, L., Xia, X., 2013. Tectonics of the North Qilian orogen, NW China. Gondwana Research 23, 1378–1401.

Staisch, L.M., Niemi, N.A., Clark, M.K., Chang, H., 2016. Eocene to late Oligocene history of crustal shortening within the Hoh Xil Basin and implications for the uplift history of the northern Tibetan Plateau. Tectonics 35, 862–895.

Sun, B., Wang, Y.F., Li, C.S., Yang, J., Li, J.F., Li, Y.L., Deng, T., Wang, S.Q., Zhao, M., Spicer, R.A., Ferguson, D.K., Mehrotra, R.C., 2015. Early Miocene elevation in northern Tibet estimated by palaeobotanical evidence. Scientific Reports 5, 10379.

Tapponnier, P., Xu, Z., Roger, F., Meyer, B., Arnaud, N., Wittlinger, G., Yang, J., 2001. Oblique stepwise rise and growth of the Tibet Plateau. Science 294, 1671–1677.

Taylor, M., Yin, A., 2009. Active structures of the Himalayan-Tibetan orogen and their relationships to earthquake distribution, contemporary strain field, and Cenozoic volcanism. Geosphere 5, 199–214.

Van Hinsbergen, D.J.J., Lippert, P.C., Dupont-Nivet, G., McQuarrie, N., Doubrovine, P.V., Spakman, W., Torsvik, T.H., 2012. Greater India Basin hypothesis and a two-stage Cenozoic collision between India and Asia. Proceedings of the National Academy of Sciences 109, 7659–7664.

Vermeesch, P., 2009. RadialPlotter: a Java application for fission track, luminescence and other radial plots. Radiation Measurements 44, 409–410.

Volkmer, J.E., Kapp, P., Guynn, J.H., Lai, Q., 2007. Cretaceous-Tertiary structural evolution of the north central Lhasa terrane, Tibet. Tectonics 26, TC6007. https://doi.org/10.1029/2005TC001832.

Wang, C., Zhao, X., Liu, Z., Lippert, P.C., Graham, S.A., Coe, R.S., Yi, H., Zhu, L., Liu, S., Li, Y., 2008. Constraints on the early uplift history of the Tibetan Plateau. Proceedings of the National Academy of Sciences 105, 4987–4992.

Wang, Y., Zheng, J., Zheng, Y., Liu, X., Sun, G., 2015. Paleocene-Early Eocene uplift of the Altyn Tagh Mountain: evidence from detrital zircon fission track analysis and seismic sections in the northwestern Qaidam basin. Journal of Geophysical Research - Solid Earth 120, 8534–8550.

Wang, F., Feng, H., Shi, W., Zhang, W., Wu, L., Yang, L., Wang, Y., Zhang, Z., Zhu, R., 2016. Relief history and denudation evolution of the northern Tibet margin: constraints from $^{40}Ar/^{39}Ar$ and (U–Th)/He dating and implications for far-field effect of rising plateau. Tectonophysics 675, 196–208.

Wang, W., Zhang, P., Pang, J., Garzione, C., Zhang, H., Liu, C., Zheng, D., Zheng, W., Yu, J., 2016. The Cenozoic growth of the Qilian Shan in the northeastern Tibetan Plateau: a sedimentary archive from the Jiuxi Basin. Journal of Geophysical Research - Solid Earth 121, 2235–2257.

Wang, X., Song, C., Zattin, M., He, P., Song, A., Li, J., Wang, Q., 2016. Cenozoic pulsed deformation history of northeastern Tibetan Plateau reconstructed from fission-track thermochronology. Tectonophysics 672, 212–227.

Xia, W., Zhang, N., Yuan, X., Fan, L., Zhang, B., 2001. Cenozoic Qaidam basin, China: a stronger tectonic inversed, extensional rifted basin. American Association of Petroleum Geologists Bulletin 85, 715–736.

Xia, L., Li, X., Ma, Z., Xu, X., Xia, Z., 2011. Cenozoic volcanism and tectonic evolution of the Tibetan plateau. Gondwana Research 19, 850–866.

Xu, Q., Ding, L., Zhang, L., Cai, F., Lai, Q., Yang, D., Liu-Zeng, J., 2013. Paleogene high elevations in the Qiangtang Terrane, central Tibetan Plateau. Earth and Planetary Science Letters 362, 31–42.

Yin, A., Rumelhart, P.E., Butler, R.E., Cowgill, E., Harrison, T.M., Foster, D.A., Ingersoll, R.V., Zhang, Q., Zhou, X.-Q., Wang, X.-F., Hanson, A., Raza, A., 2002. Tectonic history of the Altyn Tagh fault system in northern Tibet inferred from Cenozoic sedimentation. Geological Society of America Bulletin 114, 1257–1295.

Yin, A., Dang, Y., Wang, L., Jiang, W., Zhou, S., Chen, X., Gehrels, G.E., McRivette, M.W., 2008a. Cenozoic tectonic evolution of Qaidam basin and its surrounding regions (part 1): the southern Qilian Shan-Nan Shan thrust belt and northern Qaidam basin. Geological Society of America Bulletin 120, 813–846.

Yin, A., Dang, Y., Zhang, M., Chen, X., McRivette, M.W., 2008b. Cenozoic tectonic evolution of the Qaidam basin and its surrounding regions (part 3): structural geology, sedimentation, and regional tectonic reconstruction. Geological Society of America Bulletin 814 (120), 847–876.

Yue, Y., Liou, J.G., 1999. Two-stage evolution model for the Altyn Tagh fault, China. Geology 27, 227–230.

Yue, Y., Ritts, B.D., Graham, S.A., Wooden, J.L., Gehrels, G.E., Zhang, Z., 2003. Slowing extrusion tectonics: lowered estimate of post-Early Miocene slip rate for the Altyn Tagh fault. Earth and Planetary Science Letters 217, 111–122.

Zhang, H.P., Zhang, P.Z., Zheng, D.W., Zheng, W.J., Chen, Z.W., Wang, W.T., 2014. Transforming the Miocene Altyn Tagh fault slip into shortening of the northwestern Qilian Shan: insights from the drainage basin geometry. Terra Nova 26, 216–221.

Zheng, H., Powell, C.M., An, Z., Zhou, J., Dong, G., 2000. Pliocene uplift of the northern Tibetan Plateau. Geology 28, 715–718.

Zheng, D., Clark, M.K., Zhang, P., Zheng, W., Farley, K.A., 2010. Erosion, fault initiation and topographic growth of the North Qilian Shan (northern Tibetan Plateau). Geosphere 6, 937–941.

Zhou, J., Xu, F., Wang, T., Cao, A., Yin, C., 2006. Cenozoic deformation history of the Qaidam Basin, NW China: results from cross-section restoration and implications for Qinghai–Tibet Plateau tectonics. Earth and Planetary Science Letters 243, 195–210.

Zhuang, G., Hourigan, J.K., Ritts, B.D., Kent-Corson, M.L., 2011. Cenozoic multiple-phase tectonic evolution of the northern Tibetan Plateau: constraints from sedimentary records from Qaidam basin, Hexi Corridor, and Subei basin, Northwest China. American Journal of Science 311, 116–152.

Zhuang, G., Johnstone, S., Hourigan, J., Lippert, P.C., Ritts, B., Robinson, A.C., Sobel, E.R., 2018. Understanding the geologic evolution of northern Tibetan Plateau with multiple thermochronometers. Gondwana Research 58, 195–210.